

# Belief Propagation Decoding of Quantum LDPC Codes with Guided Decimation

Hanwen Yao<sup>1,2</sup>, Waleed Abu Laban<sup>3</sup>, Christian Häger<sup>3</sup>,

Alexandre Graell i Amat<sup>3</sup>, and Henry D. Pfister<sup>1,2,4</sup>

<sup>1</sup>Duke Quantum Center, Duke University, Durham, NC, USA

<sup>2</sup>Dept. of Electrical and Computer Engineering, Duke University, Durham, NC, USA

<sup>3</sup>Dept. of Electrical Engineering, Chalmers University of Technology, Gothenburg, Sweden

<sup>4</sup>Dept. of Mathematics, Duke University, Durham, NC, USA

## Abstract

Quantum low-density parity-check (QLDPC) codes have emerged as a promising technique for quantum error correction. A variety of decoders have been proposed for QLDPC codes and many of them utilize belief propagation (BP) decoding in some fashion. However, the use of BP decoding for degenerate QLDPC codes is known to face issues with convergence. These issues are commonly attributed to short cycles in the Tanner graph and multiple syndrome-matching error patterns due to code degeneracy. Although various methods have been proposed to mitigate the non-convergence issue, such as BP with ordered statistics decoding (BP-OSD) and BP with stabilizer inactivation (BP-SI), achieving better performance with lower complexity remains an active area of research.

In this work, we propose to decode QLDPC codes with BP guided decimation (BPGD), which has been previously studied for constraint satisfaction and lossy compression problems. The decimation process is applicable to both binary BP and quaternary BP and involves sequentially freezing the value of the most reliable qubits to encourage BP convergence. Despite its simplicity, we find that BPGD significantly reduces BP failures due to non-convergence while maintaining a low probability of error given convergence, achieving performance on par with BP-OSD and BP-SI. To better understand how and why BPGD improves performance, we discuss several interpretations of BPGD and their connection to BP syndrome decoding.

# 1 Introduction

In a quantum computing system, error correction is an essential building block to protect fragile quantum information against decoherence and other noise sources. The general framework of quantum stabilizer codes has been studied extensively [1–3]. Using this framework, various quantum error-correcting codes have been constructed over the past two decades including toric codes [4, 5], surface codes [6–10], and various quantum low-density parity-check (QLDPC) codes [11–17]. Among them, QLDPC codes provide a promising direction because they can support multiple logical qubits and their low-weight stabilizers allow reliable syndrome measurement in practice. Until recently, researchers did not know how to construct QLDPC codes with constant rate and linear distance. But, in a series of recent advances [18–21], researchers have overcome this obstacle and there are now constructions of asymptotically *good* quantum LDPC codes with constant rate and linear minimum distance.

In classical communication, low-density parity-check (LDPC) codes were first proposed by Gallager [22] in 1962 and are now widely applied in practical communication systems [23, 24]. LDPC codes are typically decoded with the belief propagation (BP) algorithm [25], which has low complexity and can provide good performance for code rates close to the channel capacity [26–29]. However, in the quantum scenario, the performance of BP decoding based on syndrome measurement is hindered by cycles in the Tanner graph and code degeneracy. The first problem follows from the commutativity constraint imposed on stabilizer codes which produces unavoidable cycles in the Tanner graph that degrade the BP decoding performance [30, 31]. The second is because good QLDPC codes are recognized to be highly *degenerate*; this means that their minimum distance is much larger than the minimum weight of their stabilizers. Due to degeneracy, the syndrome (i.e., stabilizer measurements) can be used to identify a correction procedure that works with high probability even when the actual error is not uniquely identified. This hinders convergence of the BP decoding process [30, 32].

Since the initial application of BP to decode QLDPC codes by Poulin and Chung [30], significant efforts have been made to enhance its performance. Various methods have been proposed to modify the BP decoding process itself, including random perturbation [30], enhanced feedback [33], grouping check nodes as super nodes [31], parity-check matrix augmentation [34], neural BP [35–37], generalized BP [38], and adaptive BP with memory [39]. Alternatively, post-processing methods have also been explored to improve

performance. In [16], when BP fails to converge, it was proposed to use ordered statistics decoding (OSD) to construct a syndrome-matching error pattern based on the soft information provided by BP. This is called the BP-OSD algorithm. Another post-processing approach introduced in [40] involves iteratively running BP with stabilizer inactivation (BP-SI).

In this work, we propose to improve the BP decoding performance for QLDPC codes by combining it with guided decimation. The term “decimation” refers to the process of sequentially fixing variables to hard decisions during iterative decoding [41, 42]. In our proposed belief propagation guided decimation (BPGD) algorithm, we incorporate this method by sequentially freezing the most reliable qubit based on its soft information after a certain number of BP iterations. Despite its simplicity, we show that BPGD outperforms both BP-OSD with order 0 and BP-SI with 10 inactivated stabilizers under independent Pauli- $\sigma_x$  errors. Notably, BPGD exhibits lower complexity than BP-OSD and comparable complexity to BP-SI, without the need to solve any systems of linear equations.

The BPGD algorithm was first shown to work well for  $K$ -SAT constraint satisfaction [42, 43] and lossy compression problems [44, 45]. A variation has also been shown to improve the neural BP performance for classical LDPC codes [46]. To better understand how guided decimation improves BP performance for QLDPC codes, we discuss some interpretations of BPGD and their connection to the BP syndrome decoding problem for the stabilizer codes. Additionally, through a randomized version of BPGD, we shed light on how code degeneracy contributes to the non-convergence issue in syndrome BP decoding over QLDPC codes. Our experiment also shows that guided decimation improves BP convergence, and highlights how BPGD benefits from code degeneracy. Furthermore, we extend BPGD from binary symbols to quaternary symbols, demonstrating competitive performance compared to BP-OSD in the high-error-rate regime under depolarizing noise.

## 2 Preliminaries

### 2.1 Binary Linear Codes

Let  $\mathbb{F}_2 = \{0, 1\}$  be the binary Galois field defined by modulo-2 addition and multiplication. A length- $n$  binary linear code  $\mathcal{C} \subseteq \mathbb{F}_2^n$  is a subset of length- $n$  binary strings satisfying  $w + x \in \mathcal{C}$  for all  $w, x \in \mathcal{C}$ . Such

a code forms a vector space over  $\mathbb{F}_2$ . A generator matrix  $G \in \mathbb{F}_2^{k \times n}$  for  $\mathcal{C}$  is a  $k \times n$  matrix whose rows span the code. A parity-check matrix  $H \in \mathbb{F}_2^{(n-k) \times n}$  for  $\mathcal{C}$  is an  $(n-k) \times n$  matrix whose rows are orthogonal to the code.

For communication where the codeword  $x \in \mathcal{C}$  is corrupted by an additive error vector  $z \in \mathbb{F}_2^n$ , the received vector is given by  $y = x + z$ . Then, the optimal recovery process for  $x$  given  $y$  is given by choosing a codeword  $\hat{x}$  that maximizes the conditional probability given  $y$ . Since  $Hx = 0$ , it follows that the syndrome vector  $s \triangleq Hy \in \mathbb{F}_2^{n-k}$  satisfies

$$s = H(x + z) = Hz. \quad (1)$$

For the binary symmetric channel (BSC) where  $z$  is an i.i.d. vector, the optimal recovery process can also be implemented by *syndrome decoding* where the syndrome  $s$  is mapped to the minimum-weight error vector in the coset  $\{u \in \mathbb{F}_2^n \mid Hu = s\}$  containing  $z$ . For more details on this well-known classical setup, see [47].

## 2.2 Stabilizer Formalism

An  $[[n, k]]$  quantum stabilizer code is an error correction code designed to protect  $k$  logical qubits with  $n$  physical qubits against noise. To establish the definition of quantum stabilizer codes, we first define the Pauli operators. For a single qubit, its pure quantum state is represented as a unit vector in the two-dimensional Hilbert space  $\mathbb{C}_2$ . The Pauli operators for a single qubit system are defined as the  $2 \times 2$  complex Hermitian matrices

$$I = \begin{bmatrix} 1 & 0 \\ 0 & 1 \end{bmatrix}, \sigma_x = \begin{bmatrix} 0 & 1 \\ 1 & 0 \end{bmatrix}, \sigma_z = \begin{bmatrix} 1 & 0 \\ 0 & -1 \end{bmatrix}, \sigma_y = i\sigma_x\sigma_z = \begin{bmatrix} 0 & -i \\ i & 0 \end{bmatrix},$$

and they form a basis for all  $2 \times 2$  complex matrices. For an  $n$ -qubit system, we are working in  $\mathbb{C}_2^{\otimes n}$ , the  $n$ -fold Kronecker product of the two-dimensional Hilbert space. Given two length- $n$  binary vectors  $a = (a_1, a_2, \dots, a_n) \in \mathbb{F}_2^n$ , and  $b = (b_1, b_2, \dots, b_n) \in \mathbb{F}_2^n$ , we define the  $n$ -fold Pauli operator  $D(a, b)$  as

$$D(a, b) = \sigma_x^{a_1} \sigma_z^{b_1} \otimes \sigma_x^{a_2} \sigma_z^{b_2} \otimes \dots \otimes \sigma_x^{a_n} \sigma_z^{b_n}. \quad (2)$$

It follows that the Pauli operators  $i^k D(a, b)$  with  $a, b \in \mathbb{F}_2^n$  and an overall phase  $i^k$  with  $k \in \{0, 1, 2, 3\}$  form the  $n$ -qubit Pauli group, denoted as  $\mathcal{P}_n$ . Since  $\sigma_x \sigma_z = -\sigma_z \sigma_x$ , the multiplication rule in this group is given by

$$D(a, b)D(a', b') = (-1)^{a'b^T + b'a^T} D(a', b')D(a, b) \quad (3)$$

$$= (-1)^{a'b^T} D(a + a', b + b'). \quad (4)$$

The *symplectic inner product* between length- $2n$  binary vectors  $(a, b)$  and  $(a', b')$  is defined by

$$\langle (a, b), (a', b') \rangle_s \triangleq (a', b') \Lambda (a, b)^T = b'a^T + a'b^T \pmod{2}, \quad \Lambda = \begin{bmatrix} 0 & I_n \\ I_n & 0 \end{bmatrix}. \quad (5)$$

It equals 0 if the two Pauli operators  $D(a, b)$  and  $D(a', b')$  commute and it is 1 if they anti-commute.

A quantum stabilizer code  $\mathcal{C}$  with  $n$  physical qubits is defined via a commutative subgroup  $\mathcal{S} \subseteq \mathcal{P}_n$  with  $-I_2^{\otimes n} \notin \mathcal{S}$ . The subgroup  $\mathcal{S}$  is referred to as the *stabilizer group*, and the Pauli operators in  $\mathcal{S}$  are called the *stabilizers*, or *checks* in the context of decoding. The code space consists of all states in  $\mathbb{C}_2^{\otimes n}$  stabilized by  $\mathcal{S}$  as follows:

$$\mathcal{C} = \{|\psi\rangle \in \mathbb{C}_2^{\otimes n} : M|\psi\rangle = |\psi\rangle, \forall M \in \mathcal{S}\}. \quad (6)$$

In other words,  $\mathcal{C}$  consists of states that are +1 eigenstates for all the stabilizers in  $\mathcal{S}$ . If  $\mathcal{S}$  has  $n - k$  independent generators, the code space has dimension  $k$ . The *weight* of a Pauli operator in  $\mathcal{P}_n$  is defined to be the number of elements in its  $n$ -fold Kronecker product that are not equal to  $I$ . The *distance* of a stabilizer code is defined as the minimum weight of all Pauli operators in  $N(\mathcal{S}) \setminus \mathcal{S}$ , where  $N(\mathcal{S})$  denotes the normalizer group of  $\mathcal{S}$  in  $\mathcal{P}$ . If code  $\mathcal{C}$  has distance  $d$ , we call  $\mathcal{C}$  an  $[[n, k, d]]$  quantum stabilizer code. In particular,  $\mathcal{C}$  is called *degenerate* if its distance  $d$  is larger than the minimum weight of its stabilizers.

In the symplectic representation, the stabilizer  $\mathcal{S}$  is constructed from the rows of the stabilizer matrix

$$H = [H_x, H_z], \quad (7)$$

where  $H_x, H_z \in \mathbb{F}_2^{m \times n}$  are binary matrices with  $m$  rows and  $n$  columns. In particular, each row  $(h_x, h_z)$

of  $H$  defines the stabilizer  $D(h_x, h_z)$  and the set of stabilizers defined by all rows generates the stabilizer group  $\mathcal{S}$ . In this way, the constraint requiring all the stabilizers in  $H$  to commute with each other can be expressed as  $H\Lambda H^T = H_x H_z^T + H_z H_x^T = 0$ . There is an important class of stabilizer codes, known as Calderbank–Shor–Steane (CSS) codes [48, 49], where each stabilizer has the form  $D(a, 0)$  (i.e., only  $\sigma_x$  operators) or  $D(0, b)$  (i.e., only  $\sigma_z$  operators). In this case, we have

$$H_x = \begin{bmatrix} 0 \\ G_2 \end{bmatrix}, \quad H_z = \begin{bmatrix} H_1 \\ 0 \end{bmatrix}, \quad (8)$$

where  $H_1 \in \mathbb{F}_2^{(n-k_1) \times n}$  is the parity-check matrix of a classical  $[n, k_1]$  code  $\mathcal{C}_1$  and  $G_2 \in \mathbb{F}_2^{k_2 \times n}$  is the generator matrix of a classical  $[n, k_2]$  code  $\mathcal{C}_2$ . Thus, the stabilizer matrix has the form

$$H = \begin{bmatrix} 0 & H_1 \\ G_2 & 0 \end{bmatrix}. \quad (9)$$

For CSS codes, the commutativity constraint for the stabilizers, which is given by  $H\Lambda H^T = 0$ , reduces to  $G_2 H_1^T = 0$  which is equivalent to  $\mathcal{C}_2 \subseteq \mathcal{C}_1$ . In this work, we will focus our discussion on the CSS codes.

### 2.3 Syndrome Decoding of Stabilizer Codes

While classical codes are typically decoded from direct observations of the received sequence, directly measuring qubits in a stabilizer code may destroy the entanglement (or superposition) in the quantum state. To avoid this, one instead measures whether or not certain stabilizers commute with the quantum state. These measurements reveal the syndrome of the error that occurred and then syndrome decoding can be used to identify the best method to correct the error.

For an  $[[n, k]]$  stabilizer code  $\mathcal{C}$ , we will consider two error models in this work. The first model is the independent Pauli- $\sigma_x$  error channel, where each encoded qubit is independently affected by a Pauli- $\sigma_x$  error with a probability  $p_x$ . For this model, we will discuss the binary version of our algorithm. The second model is the *depolarizing channel* characterized by a physical error rate  $p$ . In this model, each encoded qubit is independently affected by Pauli  $\sigma_x$ ,  $\sigma_y$ , or  $\sigma_z$  errors, each with probability  $p/3$ . For the depolarizing

channel, we will discuss the quaternary version of our algorithm.

In both of these models, the encoded state  $|\psi\rangle$  is corrupted by an  $n$ -qubit Pauli error  $E = D(x, z) \in \mathcal{P}_n$  as  $|\psi\rangle \rightarrow E|\psi\rangle$ . For the decoder, the goal is to detect and correct this error by conducting measurements on all the stabilizers in the parity-check matrix  $H$ . The measurement result can be expressed as the symplectic inner product  $\langle (a, b), (x, z) \rangle_s$  for a particular stabilizer  $M = D(a, b) \in \mathcal{S}$ , indicating whether  $E$  commutes or anti-commutes with  $M$ . The symplectic inner product of the Pauli error  $(x, z)$  with the stabilizers in  $H$  form the length- $m$  binary syndrome vector

$$s = (x, z)\Lambda H^T. \quad (10)$$

This succinctly encapsulates all the information derived from the measurements. For CSS codes,  $H_1$  defines  $\sigma_z$ -stabilizers that interact with Pauli- $\sigma_x$  errors and  $G_2$  defines  $\sigma_x$ -stabilizers that interact with Pauli- $\sigma_z$  errors. Thus, we can separate the length  $m = n - k_1 + k_2$  syndrome vector into two parts  $s = (s_x, s_z)$  where  $s_x = xH_1^T$  has length  $n - k_1$  and  $s_z = zG_2^T$  has length  $k_2$ . In this work, we assume that all syndrome measurements are perfect.

Based on its syndrome, the Pauli error  $E$  that affects the qubits can be categorized as follows:

1. **Detectable Error:**  $E$  is called *detectable* if its syndrome  $s$  is not the all-one vector. In other words,  $E$  is detectable if it anticommutes with at least one of the stabilizers in  $\mathcal{S}$ . Otherwise,  $E$  is called *non-detectable*.
2. **Degenerate Error:** If  $E$  is a non-detectable error, it is called *degenerate* if it belongs to the stabilizer group, i.e.,  $E \in \mathcal{S}$ . In this case,  $E$  preserves the encoded state and needs no correction.
3. **Logical Error:** If  $E$  is a non-detectable error that does not belong to the stabilizer group, i.e.,  $E \in N(\mathcal{S}) \setminus \mathcal{S}$ , it is called a *logical* error, and it alters the logical state of the encoded qubits.

After obtaining the syndrome  $s$  through measurement, the task of the decoder is to find an estimated  $\widehat{E}$  with the same syndrome. Then, the reverse operator  $\widehat{E}^\dagger$  can be applied to the affected qubits as  $E|\psi\rangle \rightarrow \widehat{E}^\dagger E|\psi\rangle$  for error correction. This decoding process has four possible outcomes:

1. **Decoding Failure:** The decoder fails to provide an estimated  $\widehat{E}$  that yields the syndrome  $s$ .

2. **Successful Decoding (Exact Match):** The estimated error is equal to the channel error, i.e.,  $\hat{E} = E$ .
3. **Successful Decoding (Degenerate Error):** The difference between the estimated error and the channel error is a degenerate error, i.e.,  $\hat{E}^\dagger E \in \mathcal{S}$ .
4. **Decoding Failure (Logical Error):** The difference between the estimated error and the channel error is a logical error, i.e.,  $\hat{E}^\dagger E \in N(\mathcal{S}) \setminus \mathcal{S}$ .

Since there are  $2^m$  possible syndromes, using a look-up table for error estimation quickly becomes infeasible as the number of qubits increases because  $m$  typically scales linearly with  $n$ . Thus, a computationally efficient decoder is required for long stabilizer codes. Now, we describe the two decoding strategies for stabilizer codes using the names from [50].

**Quantum Maximum Likelihood Decoding (QMLD):** This decoding strategy aims at finding the most probable error  $E = D(X, Z)$  given the syndrome, where  $X, Z \in \mathbb{F}_2^n$  are random vectors drawn from some Pauli error distribution. In this model, the syndrome is a random vector defined by  $S = (X, Z)\Lambda H^T$ . Given the observed syndrome event  $S = s$ , we compute  $\hat{E} = D(\hat{X}, \hat{Z})$  where

$$(\hat{X}, \hat{Z}) = \arg \max_{(x', z') \in \mathbb{F}_2^n \times \mathbb{F}_2^n} \Pr((X, Z) = (x', z') \mid S = s). \quad (11)$$

For the independent Pauli- $\sigma_x$  error channel and the depolarizing channel, solving (11) is at least as hard as the maximum-likelihood decoding problem in classical coding theory, which is well-known to be NP-complete [51].

**Degenerate Quantum Maximum Likelihood Decoding (DQMLD):** Denote the coset of the stabilizer group  $\mathcal{S}$  shifted by a Pauli error  $E \in \mathcal{P}_n$  as  $\mathcal{S}(E)$ , and denote the set of all cosets of  $\mathcal{S}$  as  $\mathcal{P}_n/\mathcal{S}$ . In the context of a stabilizer code, where all Pauli errors in the same coset  $\mathcal{S}(E)$  affect the logic state of encoded qubits equivalently, the optimal decoding strategy would be finding the most probable coset  $\mathcal{S}(E)$  given the observed syndrome event  $S = s$ . After that, the decoder can choose any error pattern  $\hat{E}$  in this coset as the error to be corrected, as the specific pattern selected does not affect the result due to degeneracy. This decoding problem has been shown to be #P-complete [50], which is computationally much harder than QMLD.



## 2.4 Syndrome Decoding for Pauli- $\sigma_x$ Errors

In Sections 3 and 4 that follow, we will focus on the syndrome decoding problem for CSS codes over the independent Pauli- $\sigma_x$  error channel with probability  $p_x$ , where the Pauli error has the form  $E = D(X, 0)$ , with  $X \in \mathbb{F}_2^n$  being a random vector following the distribution:

$$\Pr(X = (x_1, x_2, \dots, x_n)) = \prod_{i=1}^n p_x^{x_i} (1 - p_x)^{1-x_i} \quad (12)$$

In the following, we will use the random vector  $X$  to denote the channel error for simplicity. For CSS codes in this case, given  $X$ , the decoder only needs to consider part of the syndrome  $S_x = XH_1^T$ , where  $H_1$  is the submatrix of  $H_z$  as in (8). The QMLD decoding problem then becomes computing  $\hat{X}$  where

$$\hat{X} = \arg \max_{x \in \mathbb{F}_2^n} \Pr(X = x | S_x = s_x) = \arg \min_{x \in \mathbb{F}_2^n : xH_1^T = s_x} \text{wt}(x) \quad (13)$$

This is equivalent to the maximum-likelihood decoding problem for the BSC in classical coding theory, which is known to be NP-complete [51]. Thus, we turn to the low-complexity belief propagation (BP) algorithm.

## 3 Belief Propagation Decoding

BP is a low-complexity algorithm that solves inference problems for graphical models. Originated in the 1960s, Gallager's LDPC decoder [22] already contains the essence of BP, which was later formalized by Pearl in [52, 53]. In 1993, the discovery of turbo codes [54] brought along the turbo decoding algorithm, which is now recognized as an instance of BP [55]. In the late 1990s, those ideas led to the formalization of factor graphs and the sum-product algorithm [25, 56]. Among other decoders, BP is highly parallelizable for implementation, and it achieves near-optimal decoding of LDPC codes and turbo codes. It also has wide applications in other problems on graphical models, such as the spin glass models [57], lossy compression with the low-density generator matrix codes [44, 45], and constraint satisfaction problems such as  $K$ -SAT [42, 43].

BP was first introduced to the quantum decoding problem by Poulin and Chung in [30]. However, the

performance of BP for the quantum syndrome decoding problem for the QLDPC codes is degraded due to degeneracy [30, 32]. In this section, we first review the binary BP algorithm for syndrome decoding of stabilizer codes over independent Pauli- $\sigma_x$  errors. Then, we discuss some prior improvements for BP that mitigate the non-convergence problem, including BP-OSD and BP-SI.

### 3.1 Belief Propagation Syndrome Decoding for Pauli- $\sigma_x$ Errors

BP is an iterative message-passing algorithm that provides an estimate of the marginal probability  $\Pr(X_i = x_i | S_x = s_x)$  for all  $i \in [n]$ . To run BP for the syndrome decoding problem of stabilizer codes over independent Pauli- $\sigma_x$  errors with probability  $p_x$ , we first need to construct a Tanner graph  $G = (V, C, E)$  representing  $H_1$ , where  $H_1$  is the binary matrix with  $m$  rows and  $n$  columns as shown in (8). In this Tanner graph, the variable nodes in  $V = \{v_1, \dots, v_n\}$  represent the elements of  $X = (X_1, \dots, X_n)$  and the check nodes in  $C = \{c_1, \dots, c_m\}$  represent the  $\sigma_z$ -stabilizers in  $H_1$ . A variable node  $v_i$  is connected to a check node  $c_j$  if  $H_1(i, j) = 1$ . In addition, each variable node is connected to a degree 1 check node that represents the source of the channel message, and each check node is connected to a degree 1 variable node that represents the source of a syndrome bit. An example Tanner graph representing  $H_1$  for the  $[[7, 1, 3]]$  Steane code [49] with

$$H_1 = \begin{bmatrix} 1 & 1 & 1 & 0 & 1 & 0 & 0 \\ 0 & 1 & 1 & 1 & 0 & 1 & 0 \\ 0 & 0 & 1 & 0 & 1 & 1 & 1 \end{bmatrix} \quad (14)$$

is shown in Figure 1.

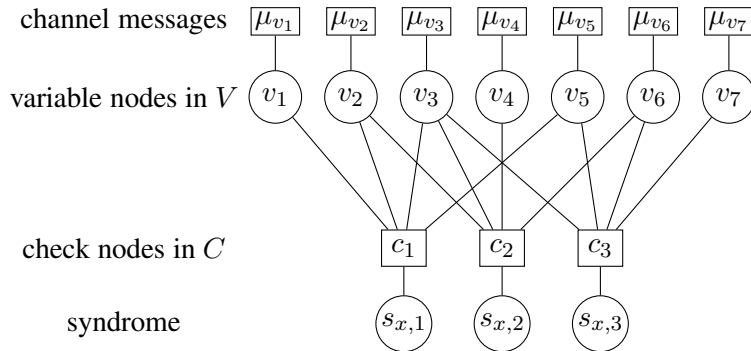


Figure 1: Tanner graph for  $H_1$  for the  $[[7, 1, 3]]$  Steane code

Let  $\mu_{v_i}$  denote the channel log-likelihood ratio (LLR) for  $v_i$  as

$$\mu_{v_i} = \log \frac{\Pr(X_i = 0)}{\Pr(X_i = 1)} = \log \frac{1 - p_x}{p_x}. \quad (15)$$

This is the initial estimate of the overall LLR of  $X_i$ . At iteration  $t = 0$ , set the message from each variable node  $v_i$  to all its connected check node  $c_j$  as

$$m_{v_i \rightarrow c_j}^{(0)} = \mu_{v_i}.$$

Then, for iteration  $t = 0, 1, \dots, T$ , given the syndrome  $s_x = (s_{x,1}, \dots, s_{x,m})$ , the messages between variable nodes and check nodes are updated as

$$m_{c_j \rightarrow v_i}^{(t)} = (-1)^{s_{x,j}} \tanh^{-1} \left( \tanh \prod_{v_k \in \partial c_j \setminus v_i} m_{v_k \rightarrow c_j}^{(t)} \right), \quad (16)$$

and

$$m_{v_i \rightarrow c_j}^{(t+1)} = \mu_{v_i} + \sum_{c_k \in \partial v_i \setminus c_j} m_{c_k \rightarrow v_i}^{(t)}, \quad (17)$$

where  $s_{x,j} \in \{0, 1\}$  is the syndrome of the  $\sigma_z$ -stabilizer corresponding to  $c_j$  (i.e., defined by the  $j$ -th row of  $H_1$ ),  $\partial c_j$  denotes the set of variable nodes in  $V$  connected to  $c_j$ , and  $\partial v_i$  denotes the set of check nodes in  $C$  connected to  $v_i$ . This update rule is called the sum-product algorithm [25]. The *bias* for variable node  $v_i$  after  $t$  iterations can be computed as

$$m_{v_i}^{(t)} = \mu_{v_i} + \sum_{c_k \in \partial v_i} m_{c_k \rightarrow v_i}^{(t)}. \quad (18)$$

For sufficiently large  $t$ , one approximates the log-likelihood ratio of the marginal probabilities for  $X_i$  with

$$m_{v_i}^{(t)} \approx \log \frac{\Pr(X_i = 0 | S_z = s_z)}{\Pr(X_i = 1 | S_z = s_z)}. \quad (19)$$

This approximation is exact if the Tanner graph  $G$  is a tree [25]. The sign of the bias  $m_{v_i}^{(t)}$  represents the hard value toward which this variable node  $v_i$  is biased, and the absolute value of the bias denoted as

$\gamma^{(t)}(v_i) = |m_{v_i}^{(t)}|$ , or just  $\gamma(v_i)$  if  $t$  is clear from the context, represents the *reliability* of this variable node. The larger the reliability, the more certain we are about its indicated hard value.

BP for syndrome decoding is commonly equipped with the following termination rule upon convergence [30]. After  $t$  iterations, the estimated hard value for  $X_i$  can be computed as

$$\hat{x}_i^{(t)} = \begin{cases} 0, & m_{v_i}^{(t)} > 0 \\ 1, & m_{v_i}^{(t)} \leq 0 \end{cases}. \quad (20)$$

The BP algorithm terminates early if the computed hard values  $\hat{x}^{(t)} = (\hat{x}_1^{(t)}, \hat{x}_2^{(t)}, \dots, \hat{x}_n^{(t)})$  match the syndrome by satisfying  $\hat{x}^{(t)} H_1^T = s_z$ . This syndrome match event is called *convergence* [30]. The BP decoder then outputs  $\hat{E} = D(\hat{x}^{(t)}, 0)$  as the estimated error operator. If none of the estimated  $\hat{x}^{(t)}$  vectors match the syndrome when  $t$  reaches a preset maximum iteration number  $T$ , then the BP decoder reports failure due to *non-convergence*.

### 3.2 Prior Works that Mitigate the Non-Convergence Issue

BP for the syndrome decoding problem of QLDPC codes is known to have issues with convergence [30,32]. Consider the  $[[882, 24, 18 \leq d \leq 24]]$  generalized bicycle B1 code proposed in [16]. We simulated its BP decoding performance with the sum-product algorithm over independent Pauli- $\sigma_x$  errors with probability  $p_x$  and the performance can be found in the blue curve in Figure 2. In our simulation, all the block error cases that we observe are due to non-convergence.

To mitigate the non-convergence issue, Pantaleev and Kalachev [16] proposed the use of ordered statistics decoding as a post-processor when BP fails to converge. In Figure 2, the red curve shows the BP-OSD performance with order 0. In this simulation, we employ the normalized min-sum algorithm for message passing with the normalization factor  $\alpha = 0.625$ , matching the decoder in [16]. The BP-OSD decoder shows a significant performance improvement over BP and this gain has been observed across various families of quantum stabilizer codes [16,58]. However, it is important to note that OSD comes with a higher computational complexity of  $O(n^3)$  [16] compared to BP. In this work, we take BP-OSD as the primary benchmark for evaluating the performance of our proposed BPGD algorithm.

Another approach to mitigate the non-convergence issue of BP, called BP with stabilizer inactivation, is proposed by Crest, Mhalla and Savin in [40]. It starts by sorting the  $\sigma_z$ -stabilizer rows in  $H_1$  in increasing order of reliability based on BP soft information. After that, the BP algorithm is run  $\lambda$  times with exactly one of the  $\lambda$  least reliable stabilizers inactivated (i.e. punctured), with early termination upon convergence. This BP-SI approach is based on the intuition that the “stabilizer-splitting” errors [32, 40] prevent BP convergence. In Figure 2, the performance of BP-SI with  $\lambda = 10$  on the B1 code is shown in the yellow curve. The data points for the yellow curve are taken and translated directly from [40, Figure 2], where the decoder uses the serial message-passing scheduling for the normalized min-sum algorithm with normalization factor  $\alpha = 0.9$ . In [40], the worst-case complexity and the average complexity of BP-SI are claimed to be  $O(\lambda_{\max} n \log n)$  and  $O(\lambda_{\text{avg}} n \log n)$ , respectively, assuming BP has complexity  $O(n \log n)$ . Here,  $\lambda_{\max}$  represents the maximum number of inactivated stabilizers and  $\lambda_{\text{avg}}$  represents the average number of inactivated stabilizers. Notably, at the end of post-processing for both BP-OSD and BP-SI, one needs to solve a system of linear equations.

## 4 Binary Belief Propagation with Guided Decimation

In this work, we use BP with guided decimation to mitigate the non-convergence issue of standard BP for QLDPC codes. The BPGD algorithm has two alternating phases:

1. iterative message-passing updates in BP to compute marginal probability approximations for the variable nodes, and
2. decimation, where we update the channel LLR of the most reliable variable node to freeze its value.

### 4.1 Message-Passing Decoding with Decimation

Message-passing algorithms with “decimation” were first introduced for the  $K$ -SAT constraint satisfaction problem based on insights from statistical physics [41]. In such problems, there are typically many valid solutions and the goal is to find just one of them. The problem is that the set of solutions can fragment into many clusters that are well separated from each other in Hamming space. When this happens, the BP algorithm does not converge to one of the solutions but instead provides information about the average of a

bit value over all valid solutions. For example, a bit message is expected to be uninformative (i.e.,  $m_{v_i}^{(t)} \approx 0$ ) if bit- $i$  is 0 in half of the solutions and 1 in the other half. But, if the bit message is highly biased towards 1 (i.e.,  $m_{v_i}^{(t)} \ll 0$ ), then bit- $i$  is expected that it takes the value 1 in a large fraction of the valid solutions. In that case, decimating (i.e., forcing) the bit value to 1 should not reduce the set of accessible valid solutions by too much and the process can continue. In [41], decimation was first combined with a related message-passing algorithm called survey propagation. Survey propagation is designed to average over the clusters in an improved manner that accounts for the fact that valid solutions often have bits that are unconstrained.

Later, the idea of decimation was extended to define the BP guided decimation (BPGD) algorithm [42] and related approaches were applied to the lossy compression problem [44, 45]. For the simplest instance of this problem, a uniform random binary source vector is quantized to a codeword in a binary linear code. The goal is to find a codeword close to the source vector or, ideally, the closest codeword. If the decoding process finds any codeword, then decoding succeeds and the cost is given by the Hamming distance to the source vector. Otherwise, the decoding process fails. The decoding and decimation process is designed to minimize the average cost. During each round of decoding and decimation, there is a natural lower bound on the cost given by minimizing over all codewords matching the current set of decimated bits. This lower bound is non-decreasing as the rounds progress and a good short-term goal for the decimation process is to make hard decisions that preserve a large number of codewords that are relatively close to the source vector. This again leads to the rule of decimating bits whose messages are strongly biased towards 0 or 1.

## 4.2 Intuition Behind BPGD for Quantum Decoding

Now, we discuss some intuitions for applying BPGD for the quantum degenerate decoding problem. In [42], the BPGD algorithm is understood to approximate the process of sampling a vector from the distribution implied by the Tanner graph. From Figure 1, we see that the Tanner graph for BP syndrome decoding constrains the error vector to match the observed syndrome and assumes each error bit is drawn independently with probability  $p_x$ .

Applying this picture to the quantum decoding problem, we can think of BPGD decoding as sampling from the error patterns that match the syndrome with weights proportional to the distribution in (12). While this type of decoding is not equivalent to either QMLD or DQMLD, we will argue that the sampling approach

is closer in spirit to DQMLD than QMLD. The reason is that the sampling probability for a correction operator is proportional to the sum of the probabilities of all the error patterns associated with that correction operator. Thus, the error is more likely to be corrected. On the other hand, QMLD tries only to find the error pattern with the highest individual probability.

### 4.3 The BPGD Algorithm

Now, the BPGD algorithm is described in detail. First, the channel LLRs for all  $v_i$  variable nodes in the Tanner graph are initialized like the BP algorithm to  $\mu_{v_i} = \log((1 - p_x)/p_x)$ . Then, decoding proceeds in rounds. In the  $r$ -th round, the BP algorithm is run for  $T$  iterations following (16) and (17). If the BP algorithm converges to an error pattern matching the syndrome, then the decoder terminates and returns the hard values of the variable nodes as the estimated error. Otherwise, the current estimated error pattern does not match the syndrome, and out of all the variable nodes that are not yet decimated, the variable node  $v_i$  with the largest reliability  $\gamma(v_i)$  is decimated by updating its channel message  $\mu_{v_i}$  based on its bias  $m_{v_i}^{(rT)}$  to

$$\mu_{v_i} = \begin{cases} \text{llr}_{\max}, & \text{if } m_{v_i}^{(rT)} > 0 \\ -\text{llr}_{\max}, & \text{if } m_{v_i}^{(rT)} \leq 0, \end{cases} \quad (21)$$

where  $\text{llr}_{\max}$  is a large fixed number. If we choose  $\text{llr}_{\max}$  to be infinity (i.e.  $\text{llr}_{\max} = \infty$ ), this decimation effectively assigns a hard value for the variable node  $v_i$  based on its bias. While letting  $\text{llr}_{\max}$  to be infinity makes sense in theory, this can also introduce numerical problems in software implementation, and thus setting  $\text{llr}_{\max}$  to be a large fixed number (e.g.  $\text{llr}_{\max} = 25$ ) is preferred in practice.

After decimating the most reliable variable node, the process starts round  $r + 1$  and the process continues either until the estimated error pattern matches the syndrome or all the variable nodes have been decimated. After all variable nodes are decimated, if the hard values of their biases still don't match the syndrome, then this is called a *non-convergence failure* of the BPGD algorithm. The pseudo-code for the BPGD algorithm is given in Algorithm 1.

---

**Algorithm 1:** Binary belief propagation with guided decimation (BPGD) over Pauli- $\sigma_x$  errors

---

**Input:** Tanner graph  $G = (V, C, E)$  for  $H_1$ , block length  $n$ , syndrome  $s_x$ , Pauli- $\sigma_x$  error rate  $p_x$ , number of iterations per round  $T$

**Output:**  $\hat{E}$  or non-convergence

- 1  $\mu_{v_i} = \log((1 - p_x)/p_x)$  for all  $v_i \in V$
- 2  $m_{v_i \rightarrow c_j}^{(0)} = \mu_{v_i}$  for all  $v_i \in V, c_j \in \partial v_i$  // BP initialization
- 3  $V_u = V$  // the set of undecimated variable nodes
- 4 **for**  $r = 1$  **to**  $n$  **do**
- 5     run  $T$  iterations of BP with the sum-product algorithm
- 6      $\hat{x} \leftarrow$  hard values for the variable nodes
- 7     **if**  $\hat{x}H_1^T = s_x$  **then**
- 8         **return**  $\hat{E} = D(\hat{x}, 0)$
- 9     **else**
- 10          $v_i = \arg \max_{v \in V_u} \gamma(v_i)$  // Pick the most reliable node in  $V_u$
- 11         **if**  $m_{v_i}^{(rT)} \geq 0$  **then**
- 12              $\mu_{v_i} = \text{llr}_{\max}$
- 13         **else**
- 14              $\mu_{v_i} = -\text{llr}_{\max}$
- 15              $V_u = V_u \setminus \{v_i\}$
- 16 **return** *non-convergence*

---

#### 4.4 Numerical Results

In Figure 2, we show the simulation result of the BPGD decoder for the  $[[882, 24, 18 \leq d \leq 24]]$  B1 code [16] over independent Pauli- $\sigma_x$  errors with probability  $p_x$ . In our software implementation of Algorithm 1, we set  $\text{llr}_{\max} = 25$ . BPGD with  $T = 100$ , shown by the green curve, yields the best performance. Using  $T = 100$  ensures that in each round, BP is run for a sufficient number of iterations to provide accurate approximate marginal probabilities for the variable nodes. Reducing the number of BP iterations per round from  $T = 100$  to  $T = 10$ , shown by the purple curve, does not significantly degrade the BPGD performance. It is worth noting that, in our simulations, the majority of the errors (over 90%) from the BPGD runs for both  $T = 100$  and  $T = 10$  are attributed to non-convergence. Therefore, similar to the BP algorithm, we rarely encounter logical errors upon convergence from running BPGD. For comparison, Figure 3 also includes the decoding performance of BP, BP-OSD with order 0, and BP-SI with  $\lambda = 10$ , whose settings are explained in Section 3.2.

In Figure 3, we also show the performance of BPGD with  $T = 10$  for the  $[[1922, 50, 16]]$  C2 code



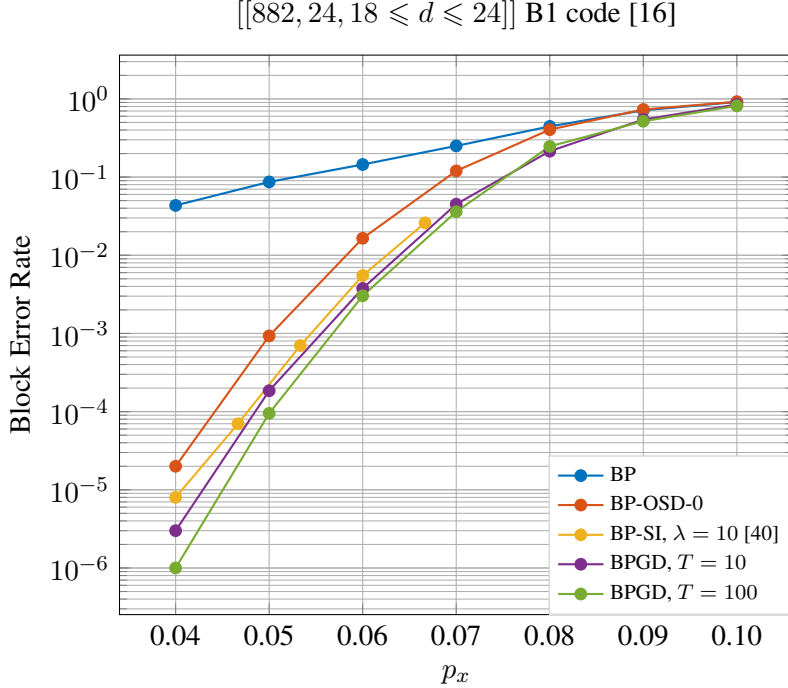


Figure 2: Performance of B1 code [16] over independent Pauli- $\sigma_x$  errors.

proposed in [16] over independent Pauli- $\sigma_x$  errors with probability  $p_x$ . For this simulation, we again set  $\text{llr}_{\max} = 25$  in Algorithm 1. For comparison, we include the performances for BP, BP-OSD with order 0, and BP-SI with  $\lambda = 10$ , whose respective settings remain consistent with those in Figure 2: 1) the BP decoder runs the basic sum-product algorithm; 2) the BP-OSD decoder with order 0 runs the serial normalized min-sum algorithm with normalization factor  $\alpha = 0.625$ ; 3) the BP-SI decoder with  $\lambda = 10$  runs the serial normalized min-sum algorithm with normalization factor  $\alpha = 0.9$ , whose data points are taken and translated directly from [40, Figure 2]. We can see that for the two QLDPC codes we considered in Figure 2 and Figure 3, BPGD shows better performance compared with BP-OSD with order 0, and is slightly better than BP-SI with  $\lambda = 10$  over independent Pauli- $\sigma_x$  errors.

We would like to note that, in our simulations in Figure 2 and Figure 3, we are using the basic sum-product algorithm with flooding scheduling for the message-passing updates in BPGD. The performance shown in Figure 2 and Figure 3 still has potential for further improvements by exploring alternative variants of BP including the normalized min-sum algorithm, serial scheduling [59, 60], neural belief propagation [35, 37], and belief propagation with memory [39].

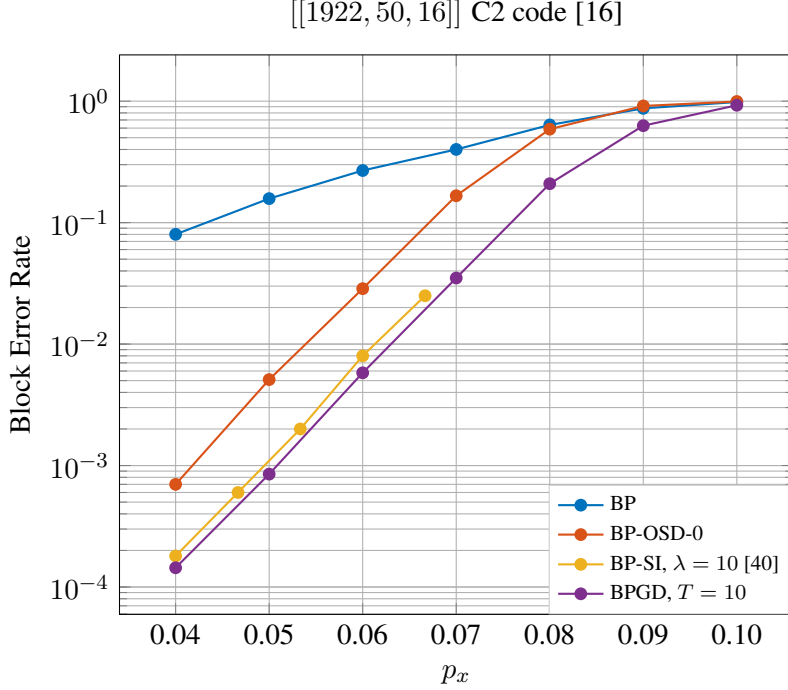


Figure 3: Performance of C2 code [16] over independent Pauli- $\sigma_x$  errors.

#### 4.5 Complexity Analysis for BPGD

BPGD requires at most  $n$  decimation rounds, each involving  $T$  iterations of message-passing updates of complexity  $O(n)$  and a search for the most reliable qubit for decimation with complexity  $O(n)$ . Therefore, the worst-case complexity of BPGD is  $O(Tn^2)$ . This worst-case complexity scales roughly the same as BP with SI [40], and it is better compared with BP-OSD with order 0, which has complexity  $O(n^3)$  [16]. Moreover, unlike BP-OSD and BP-SI, BPGD does not require solving systems of linear equations, which makes it potentially more friendly for hardware implementation.

For the BPGD algorithm, if we assume BP in each round has complexity  $O(Tn)$ , then its average-case complexity is  $O(r_{\text{avg}}Tn)$ , where  $r_{\text{avg}}$  denotes the average number of decimated variable nodes. The value of  $r_{\text{avg}}$  is highly dependent on the Pauli- $\sigma_x$  error rate  $p_x$ , meaning BPGD has different average complexity in different error rate regimes. In Table 1, we show the average number of decimated variable nodes for BPGD with  $T = 10$  when decoding the B1 code. The simulation we perform for Table 1 also produces four data points in the purple curve in Figure 2. Note that when calculating  $r_{\text{avg}}$  in Table 1, we take into account both the convergent cases and the non-convergent cases. In the case of non-convergence, the number of variable

$p_x$	0.05	0.06	0.07	0.08
simulation runs	1000000	100000	100000	10000
$r_{\text{avg}}$	2.91	9.82	60.46	231.7

Table 1: Average number of decimated variables nodes of BPGD with  $T = 10$  when decoding the B1 code [16] over Pauli- $\sigma_x$  errors.

nodes decimated by BPGD equals the block length  $n = 882$ . From Table 1 we can see that, in the low error rate regime such as  $p_x = 0.05$ ,  $r_{\text{avg}}$  becomes very small, making the average complexity of the BPGD approach  $O(Tn)$ , the complexity of the BP algorithm. We note that a similar observation has also been made for BP-SI concerning the average number of inactivated stabilizers in the low error rate regime [40]. Instead of using a fixed number  $T$  of BP iterations, if the BP algorithm is run until convergence, then it is typical to assume that  $T = O(\log n)$  iterations are required.

One natural way to reduce the worst-case complexity of BPGD is by reducing the maximum number of variable nodes it is allowed to decimate. This can be achieved by modifying line 4 in Algorithm 1 to “for  $r = 1$  to  $R$  do”, where  $R < n$  represents a predefined limit on the number of decimation rounds. With this modification, the worst-case complexity of BPGD becomes  $O(RTn)$ . In Figure 4, we present the decoding performance of BPGD with  $T = 100$  and different round limits  $R$  for the  $[[882, 24, 18 \leq d \leq 24]]$  B1 code [16]. As expected, the performance of BPGD steadily improves with increasing the round limit  $R$ . The optimal performance is attained when  $R$  is equal to the block length  $n = 882$ . This allows us to achieve a desired trade-off between worst-case complexity and the BPGD decoding performance tailored to a specific application requirement.

#### 4.6 Exploring the Role of Degeneracy with Randomized BPGD

For a degenerate QLDPC code, one reason for the non-convergence challenge faced by the BP algorithm is that, for a given syndrome, there may exist multiple low-weight error patterns that match the syndrome [30]. Note that because of degeneracy, many of those error patterns differ only by a stabilizer. Intuitively, this is supposed to help the decoder, as it essentially yields the same decoding result by outputting any of those answers. However, when running the BP algorithm, the locally operating algorithm can get confused about the direction to proceed, resulting in non-convergence [32]. In a case study presented in [30, Section IV. A], Poulin and Chung explored this scenario for a two-qubit stabilizer code. A more comprehensive study of this

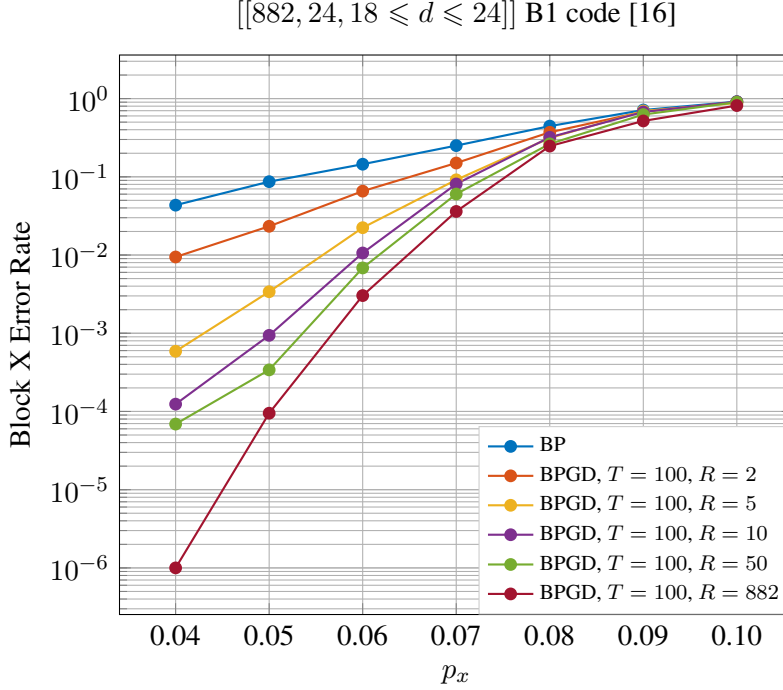


Figure 4: Performance of B1 code [16] under BPGD decoders with different decimation round limits  $R$  over independent Pauli- $\sigma_x$  errors.

phenomenon from the perspective of trapping sets can be found in the work by Raveendran and Vasić [32]. In another work, Kuo and Lai [39] examined this situation by regarding BP as an energy-minimization process, and explain non-convergence as being trapped in a local minimum of the energy function.

Here, we devise an experiment to shed light on this situation for the [[882, 24, 18 ≤ d ≤ 24]] B1 code [16]. Consider the following randomized version of the BPGD algorithm. In each round, instead of decimating the most reliable variable node, we first identify the top few reliable variable nodes, and then randomly select one of them for decimation. Concretely, this randomized decimation process is executed as follows. In the  $r$ -th round, denote  $V_u$  as the set of variable nodes that have not yet been decimated. After BP with  $T$  iterations, we first find the most reliable variable node in  $V_u$  and denote its reliability as  $\gamma_{\max}$ . Then, we construct a set  $P$  including all the variable nodes  $v_i \in V_u$  whose reliability satisfies  $\gamma(v_i) \geq \gamma_{\max} - \gamma'$ . Here,  $P$  is a set consisting of many selected reliable variable nodes prepared for random decimation, and  $\gamma'$  represents a positive reliability gap such that the reliability threshold for the inclusion of an  $v_i$  in  $P$  is  $\gamma_{\max} - \gamma'$ . Note that  $|P| \geq 1$  since  $P$  always includes the most reliable variable node in  $V_u$ . After constructing  $P$ , we randomly select a variable node in  $P$  for decimation. The pseudo-code for this

---

**Algorithm 2:** Binary belief propagation with randomized guided decimation (BPGD-rd) over Pauli- $\sigma_x$  errors

---

**Input:** Tanner graph  $G = (V, C, E)$  for  $H_1$ , block length  $n$ , syndrome  $s_x$ , Pauli- $\sigma_x$  error rate  $p_x$ , number of iterations per round  $T$ , reliability gap  $\gamma'$

**Output:**  $\hat{E}$  or non-convergence

- 1  $\mu_{v_i} = \log((1 - p_x)/p_x)$  for all  $v_i \in V$
- 2  $m_{v_i \rightarrow c_j}^{(0)} = \mu_{v_i}$  for all  $v_i \in V, c_j \in \partial v_i$  // BP initialization
- 3  $V_u = V$  // the set of undecimated variable nodes
- 4 **for**  $r = 1$  **to**  $n$  **do**
- 5     run  $T$  iterations of BP with the sum-product algorithm
- 6      $\hat{x} \leftarrow$  hard values for the variable nodes
- 7     **if**  $\hat{x}H_1^T = s_x$  **then**
- 8         **return**  $\hat{E} = D(\hat{x}, 0)$
- 9     **else**
- 10          $\gamma_{\max} = \max_{v_i \in V_u} \gamma(v_i)$
- 11          $P = \{v_i \in V_u \mid \gamma(v_i) \geq \gamma_{\max} - \gamma'\}$
- 12         randomly select  $v_i$  from  $P$  // Decimate a random variable node in  $P$
- 13         **if**  $m_{v_i}^{(rT)} \geq 0$  **then**
- 14              $\mu_{v_i} = \text{llr}_{\max}$
- 15         **else**
- 16              $\mu_{v_i} = -\text{llr}_{\max}$
- 17          $V_u = V_u \setminus \{v_i\}$
- 18 **return** *non-convergence*

---

randomized BPGD algorithm, denoted as BPGD-rd, is presented in Algorithm 2. The differences between this algorithm and the BPGD in Algorithm 1 regarding the randomized decimation process are shown in lines 10-12 in Algorithm 2.

The decoding outcome of BPGD-rd is inherently non-deterministic, due to the random selection of variable nodes for decimation in each round. Therefore, this process can potentially converge to many different error patterns. Leveraging this property, we consider the following experiment for the B1 code [16]. First, we select a Pauli- $\sigma_x$  error pattern denoted as  $E_x = D(x, 0)$ , with  $\text{wt}(E_x) = 73$ . This error pattern is randomly generated through an independent Pauli- $\sigma_x$  error channel with  $p_x = 0.08$ . Then, we run the BPGD-rd algorithm 10000 times to decode the syndrome of  $E_x$  over the Pauli- $\sigma_x$  errors, each with a distinct seed for the random decimation process. The configuration for BPGD-rd during this experiment includes  $T = 10$  for the number of BP iterations per round,  $p_x = 0.08$  for the Pauli- $\sigma_x$  error probability,  $\text{llr}_{\max} = 25$ , and  $\gamma' = 1.0$  for the reliability gap.

index	frequency	weight	distance to $E_x$	index	frequency	weight	distance to $E_x$
1	2944	73	22	6	110	73	26
2	2727	73	26	7	91	73	16
3	1560	73	20	8	68	73	20
4	1521	73	16	9	66	73	24
5	125	73	30	10	32	75	28

Table 2: A list of 10 most frequent error patterns obtained out of 10000 BPGD-rd decoding runs for the B1 code [16] for a Pauli- $\sigma_x$  error  $E_x$  of weight 73.

We observe that out of those 10000 BPGD-rd decoding runs, 9568 of them result in convergence. Within these 9568 convergent cases, we identify a total of 111 distinct error patterns, whose weights range from 73 to 87. Table 2 shows the 10 most frequent error patterns along with their weights and distances relative to the channel error  $E_x$ . Notably, all 111 error patterns differ from  $E_x$  by a stabilizer, which means that all the convergent cases decode the syndrome successfully due to degeneracy. If we run the original BPGD algorithm in Algorithm 1 to decode the syndrome of  $E_x$ , it converges to the error pattern with index 2 in Table 2.

The significance of this experiment is two-fold: On one hand, we show that for the syndrome decoding problem of a degenerate QLDPC code such as the B1 code, there can be multiple low-weight error patterns that all match the input syndrome, confusing the BP decoding process. In particular, for decoding  $E_x$  in this experiment, BP itself with the sum-product algorithm would indeed have resulted in non-convergence. On the other hand, we also show that by combining BP with guided decimation, we can break the symmetry and force convergence towards one of those error patterns as the decoding output. In this case, degeneracy plays to our advantage since decoding is successful no matter which of 111 error patterns is the winner.

Here we make some additional remarks regarding this experiment. Firstly, it can be observed that the distribution of the error patterns upon convergence in the BPGD-rd algorithm is not uniform. We can see from Table 2 that, for the syndrome decoding problem we investigated in this experiment, a significant portion of the convergent cases focuses on four specific weight-73 error patterns, as denoted by indices 1-4 in Table 2. In comparison, the original weight-73 channel error  $E_x$  does not even appear among those 111 observed error patterns.

Secondly, we note that, due to the random decimation process inherent to BPGD-rd, the results presented in this section are the product of a single simulation run of this experiment. A repeat of the same experiment

could yield different numerical results. Additionally, the outcomes depend on the specific choice of the channel error  $E_x$ . However, we observe that the phenomenon of multiple distinct error patterns matching the input syndrome and the uneven distribution among convergent error patterns appears to be a general characteristic of the BPGD-rd algorithm.

## 5 Quaternary Belief Propagation with Guided Decimation

In this section, we discuss the syndrome decoding problem for the depolarizing channel with physical error rate  $p$ , referring to Section 2.3, and present a natural extension of the binary BPGD algorithm that gives the quaternary version. Here, we represent the Pauli error as a random quaternary vector  $Q$  with its realization  $q = (q_1, q_2, \dots, q_n) \in \{0, 1, 2, 3\}^n$ , with 0, 1, 2, 3 representing the absence of error, or the presence of a Pauli  $\sigma_x$ ,  $\sigma_y$  or  $\sigma_z$  error, respectively. We define the Pauli error represented by  $q$  as  $E(q)$ . For example,

$$E(q = (1, 0, 2, 3, 0)) = \sigma_x \otimes I \otimes \sigma_y \otimes \sigma_z \otimes I. \quad (22)$$

We also define  $x_q, z_q \in \mathbb{F}_2^n$  as the length- $n$  binary vectors such that  $E(q) = D(x_q, z_q)$ . For  $q = (1, 0, 2, 3, 0)$  in the above example, we have

$$x_q = (1, 0, 1, 0, 0), \quad z_q = (0, 0, 1, 1, 0). \quad (23)$$

For the depolarizing channel, we consider the quaternary BP (Q-BP) algorithm, first discussed in [30], that jointly decode the depolarizing noise by considering correlations between Pauli- $\sigma_x$  and Pauli- $\sigma_z$  errors. Notably, Q-BP demonstrates better performance over depolarizing noise compared with decoding Pauli- $\sigma_x$  errors and Pauli- $\sigma_z$  errors separately with binary BP, as exemplified in [16, Figure 5].

To run the Q-BP algorithm for a CSS code, we need to construct a Tanner graph  $G = (V, C, E)$  similar to the binary BP. However, here  $C$  contains check nodes representing both the  $\sigma_x$ -stabilizers in  $G_2$  and the  $\sigma_z$ -stabilizers in  $H_1$ , where  $H_1$  and  $G_2$  are submatrices of  $H_x$  and  $H_z$ , respectively, as shown in (8). An

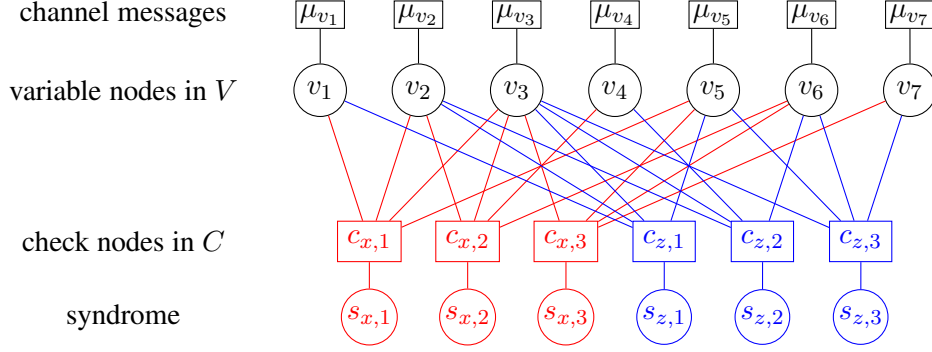


Figure 5: Tanner graph for the  $[[7, 1, 3]]$  Steane code

illustrative example for the  $[[7, 1, 3]]$  Steane code with

$$G_2 = H_1 = \begin{bmatrix} 1 & 1 & 1 & 0 & 1 & 0 & 0 \\ 0 & 1 & 1 & 1 & 0 & 1 & 0 \\ 0 & 0 & 1 & 0 & 1 & 1 & 1 \end{bmatrix} \quad (24)$$

is presented in Figure 5, where the red check nodes in  $C$  represent the  $\sigma_x$ -stabilizers, whose syndrome bits are computed as  $s_x = x_q H_1^T$ , and the blue check nodes in  $C$  represent the  $\sigma_z$ -stabilizers, whose syndrome bits are computed as  $s_z = z_q G_2^T$ .

After constructing the Tanner graph, we can run the Q-BP algorithm by iterative doing check node and variable node updates similar to the binary BP, except that the channel message  $\mu_{v_i}$  is now initialized as

$$\mu_{v_i} = (1 - p, p/3, p/3, p/3), \quad (25)$$

and each variable node  $v_i \in V$  contain the information for four probabilities  $(p_{v_i,0}, p_{v_i,1}, p_{v_i,2}, p_{v_i,3})$ . After a sufficient number of message-passing iterations, those four probabilities approximate the marginal probabilities for  $Q_i$  in the quaternary error vector  $Q = (Q_1, Q_2, \dots, Q_n)$  conditioned on the syndrome event  $S = s$  as

$$p_{v_i,j} \approx \Pr(Q_i = j \mid S = s), \quad \text{for } j \in \{0, 1, 2, 3\}. \quad (26)$$



With the four probabilities normalized with

$$p_{v_i,0} + p_{v_i,1} + p_{v_i,2} + p_{v_i,3} = 1, \quad (27)$$

we define the reliability for the variable node  $v_i$  as  $\gamma(v_i) = \max\{p_{v_i,0}, p_{v_i,1}, p_{v_i,2}, p_{v_i,3}\}$ . A detailed description of the message-passing updates of Q-BP and its convergence condition is available in [61] and [31]. An efficient log domain implementation of Q-BP has also been discussed in [62].

Similar to its binary counterpart, the Q-BP algorithm can also be improved by guided decimation, denoted as the quaternary belief propagation guided decimation (Q-BPGD) algorithm. After the  $T$  iterations of BP in each round, out of all the variable nodes we have not yet decimated, we pick the variable node  $v_i$  with the largest reliability  $\gamma(v_i)$  and decimate it by changing its channel message as

$$\mu_{v_i} = \begin{cases} (1 - \epsilon, \epsilon, \epsilon, \epsilon), & \text{if } \arg \max_{j \in \{0,1,2,3\}} p_{v_i,j} = 0 \\ (\epsilon, 1 - \epsilon, \epsilon, \epsilon), & \text{if } \arg \max_{j \in \{0,1,2,3\}} p_{v_i,j} = 1 \\ (\epsilon, \epsilon, 1 - \epsilon, \epsilon), & \text{if } \arg \max_{j \in \{0,1,2,3\}} p_{v_i,j} = 2 \\ (\epsilon, \epsilon, \epsilon, 1 - \epsilon), & \text{if } \arg \max_{j \in \{0,1,2,3\}} p_{v_i,j} = 3 \end{cases}. \quad (28)$$

As  $\epsilon$  approaches zero, this decimation rule fixes  $Q_i$  to one of the values among 0, 1, 2, 3 according to the bias of its corresponding variable node  $v_i$ . In our implementation, we set  $\epsilon = 1 \times 10^{-10}$  for numerical stability. We repeat this process until either convergence is reached at some round  $r$ , or until all the variable nodes have been decimated. The pseudo-code for the Q-BPGD algorithm is presented in Algorithm 3.

In Figure 6, we present simulation results for the Q-BPGD decoder with  $T = 10$  applied to the  $[[180, 10, 15 \leq d \leq 18]]$  A5 code proposed in [16], over the depolarizing noise. Figure 6 also shows the performances of the Q-BP decoder and the BP-OSD decoder with order 10 from [16, Figure 6]. For the A5 code, Q-BPGD exhibits improved performance compared to Q-BP and similar performance compared to BP-OSD with order 10.

In Figure 7, we also present the Q-BPGD performance with  $T = 10$  for the  $[[882, 48, 16]]$  B2 code [16]. The comparison includes both the Q-BP decoder and the BP-OSD decoder with order 10 from [16, Figure 2].

---

**Algorithm 3:** Quaternary belief propagation with guided decimation (Q-BPGD) over depolarizing noise

---

**Input:** Tanner graph  $G$ , block length  $n$ , syndrome  $s$ , physical error rate  $p$ , number of iterations per round  $T$

**Output:**  $\hat{E}$  or non-convergence

```

1  $\mu_{v_i} = (1 - p, p/3, p/3, p/3)$  for all  $v_i \in V$ 
2  $V_u = V$  // the set of undecimated variable nodes
3 for  $r = 1$  to  $n$  do
4   run  $T$  iterations of Q-BP
5    $\hat{q} \leftarrow$  hard values for the variable nodes
6   if  $\hat{q}$  matches the syndrome  $s$  then
7     | return  $\hat{E} = E(\hat{q})$ 
8   else
9     |  $v_i = \arg \max_{v \in V_u} \gamma(v_i)$  // Decimate the most reliable variable node
10    | in  $V_u$ 
11    | switch  $\arg \max_{j \in \{0,1,2,3\}} p_{v_i,j}$  do
12    |   | case 0 do  $\mu_{v_i} = (1 - \epsilon, \epsilon, \epsilon, \epsilon);$ 
13    |   | case 1 do  $\mu_{v_i} = (\epsilon, 1 - \epsilon, \epsilon, \epsilon);$ 
14    |   | case 2 do  $\mu_{v_i} = (\epsilon, \epsilon, 1 - \epsilon, \epsilon);$ 
15    |   | case 3 do  $\mu_{v_i} = (\epsilon, \epsilon, \epsilon, 1 - \epsilon);$ 
16    |    $V_u = V_u \setminus \{v_i\}$ 
17 return non-convergence

```

---

For the B2 code, Q-BPGD outperforms the BP-OSD decoder with order 0 in the high-error regime but is surpassed by BP-OSD in the low-error-rate regime. We remark that besides the BP-OSD performance that we have been using as the main comparison benchmark in this paper, a very good decoding performance is also reported in [39, Figure 13] for the B2 code using an adaptive version of BP with memory over the depolarizing noise.

Asymptotically, the worst-case complexity of the Q-BPGD algorithm is the same as the binary BPGD, which is  $O(Tn^2)$ . However, for moderate block lengths, Q-BPGD runs slower compared with binary BPGD, due to the computation of four probabilities  $(p_{v_i,1}, p_{v_i,2}, p_{v_i,3}, p_{v_i,4})$  for every variable node  $v_i$  in each BP iteration. Our current software implementation of Q-BPGD is slower than binary BPGD with incurring of exponential and log functions, but we expect with approximation, the running time of Q-BPGD is similar to that of binary BPGD. Furthermore, we remark that the performance of Q-BPGD shown in Figure 6 and Figure 7 are also subject to potential improvements by using other variants of Q-BP.

[[180, 10, 15 ≤ d ≤ 18]] A5 code [16]

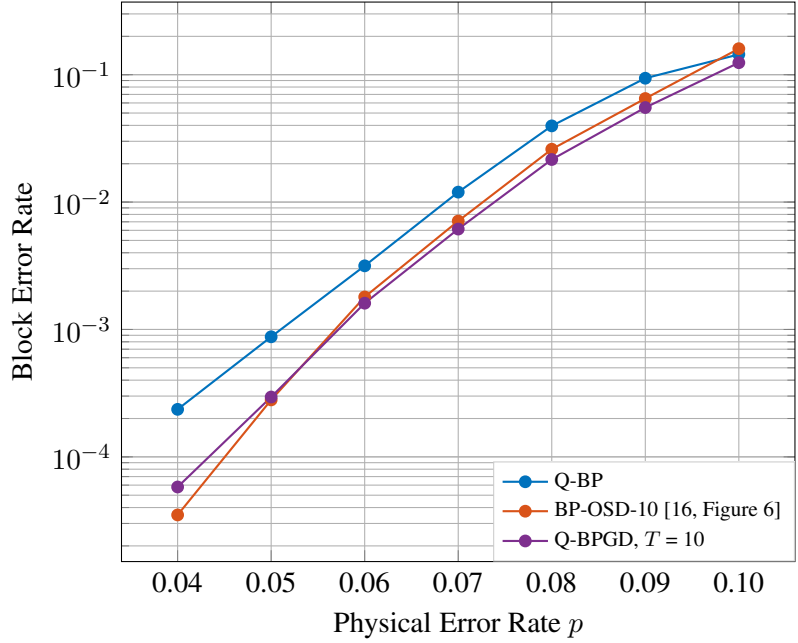


Figure 6: Performance of A5 code [16] over depolarizing noise.

## 6 Conclusion

In this paper, we have introduced and evaluated the use of BPGD for decoding QLDPC codes to encourage convergence. BPGD showed strong performance compared with BP-OSD, and BP-SI under independent Pauli- $\sigma_x$  errors. To better understand how BPGD boosts convergence, we have provided an alternative view of the BP syndrome decoding setup for stabilizer codes as a sampling problem. Furthermore, to understand the performance of BPGD for degenerate QLDPC codes, we experimented with a randomized version of BPGD that helped illuminate the role of degeneracy in syndrome decoding. Our experiments suggested that BPGD performed well because degeneracy allows it to achieve successful decoding along many different decimation paths. Furthermore, we have extended our guided decimation from binary BP to quaternary BP, demonstrating competitive performance compared to BP-OSD in the high-error-rate regime under depolarizing noise.

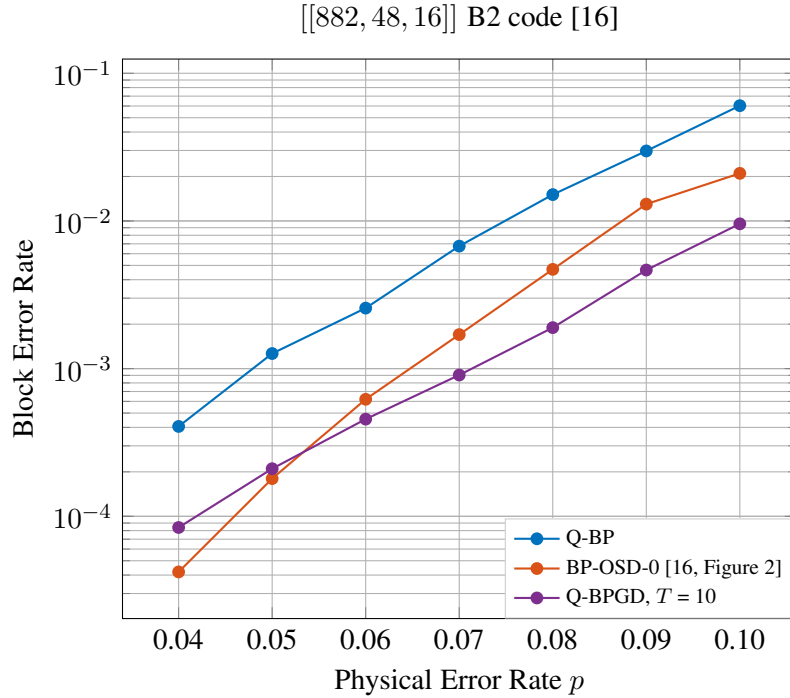


Figure 7: Performance of B2 code [16] over depolarizing noise.

## References

- [1] A. R. Calderbank, E. M. Rains, P. W. Shor, and N. J. Sloane, “Quantum error correction and orthogonal geometry,” *Physical Review Letters*, vol. 78, no. 3, p. 405, 1997.
- [2] A. R. Calderbank, E. M. Rains, P. M. Shor, and N. J. Sloane, “Quantum error correction via codes over  $GF(4)$ ,” *IEEE Transactions on Information Theory*, vol. 44, no. 4, pp. 1369–1387, 1998.
- [3] D. Gottesman, *Stabilizer codes and quantum error correction*. California Institute of Technology, 1997.
- [4] A. Y. Kitaev, “Quantum computations: algorithms and error correction,” *Russian Mathematical Surveys*, vol. 52, no. 6, p. 1191, 1997.
- [5] —, “Fault-tolerant quantum computation by anyons,” *Annals of physics*, vol. 303, no. 1, pp. 2–30, 2003.

- [6] E. Dennis, A. Kitaev, A. Landahl, and J. Preskill, “Topological quantum memory,” *Journal of Mathematical Physics*, vol. 43, no. 9, pp. 4452–4505, 2002.
- [7] M. H. Freedman, D. A. Meyer, and F. Luo, “ $Z_2$ -systolic freedom and quantum codes,” *Mathematics of quantum computation*, Chapman & Hall/CRC, pp. 287–320, 2002.
- [8] S. Bravyi, D. Poulin, and B. Terhal, “Tradeoffs for reliable quantum information storage in 2D systems,” *Physical review letters*, vol. 104, no. 5, p. 050503, 2010.
- [9] A. G. Fowler, M. Mariantoni, J. M. Martinis, and A. N. Cleland, “Surface codes: Towards practical large-scale quantum computation,” *Physical Review A*, vol. 86, no. 3, p. 032324, 2012.
- [10] D. Horsman, A. G. Fowler, S. Devitt, and R. Van Meter, “Surface code quantum computing by lattice surgery,” *New Journal of Physics*, vol. 14, no. 12, p. 123011, 2012.
- [11] D. J. MacKay, G. Mitchison, and P. L. McFadden, “Sparse-graph codes for quantum error correction,” *IEEE Transactions on Information Theory*, vol. 50, no. 10, pp. 2315–2330, 2004.
- [12] J.-P. Tillich and G. Zémor, “Quantum LDPC codes with positive rate and minimum distance proportional to the square root of the blocklength,” *IEEE Transactions on Information Theory*, vol. 60, no. 2, pp. 1193–1202, 2013.
- [13] A. A. Kovalev and L. P. Pryadko, “Improved quantum hypergraph-product LDPC codes,” in *2012 IEEE International Symposium on Information Theory Proceedings*. IEEE, 2012, pp. 348–352.
- [14] —, “Quantum kronecker sum-product low-density parity-check codes with finite rate,” *Physical Review A*, vol. 88, no. 1, p. 012311, 2013.
- [15] J. Haah, “Local stabilizer codes in three dimensions without string logical operators,” *Physical Review A*, vol. 83, no. 4, p. 042330, 2011.
- [16] P. Panteleev and G. Kalachev, “Degenerate quantum LDPC codes with good finite length performance,” *Quantum*, vol. 5, p. 585, 2021.
- [17] S. Yang and R. Calderbank, “Quantum spatially-coupled codes,” *arXiv preprint arXiv:2305.00137*, 2023.

- [18] M. B. Hastings, J. Haah, and R. O’Donnell, “Fiber bundle codes: breaking the  $N^{1/2}\text{polylog}(N)$  barrier for quantum LDPC codes,” in *Proceedings of the 53rd Annual ACM SIGACT Symposium on Theory of Computing*, 2021, pp. 1276–1288.
- [19] N. P. Breuckmann and J. N. Eberhardt, “Balanced product quantum codes,” *IEEE Transactions on Information Theory*, vol. 67, no. 10, pp. 6653–6674, 2021.
- [20] P. Panteleev and G. Kalachev, “Quantum LDPC codes with almost linear minimum distance,” *IEEE Transactions on Information Theory*, vol. 68, no. 1, pp. 213–229, 2021.
- [21] —, “Asymptotically good quantum and locally testable classical LDPC codes,” in *Proceedings of the 54th Annual ACM SIGACT Symposium on Theory of Computing*, 2022, pp. 375–388.
- [22] R. Gallager, “Low-density parity-check codes,” *IRE Transactions on information theory*, vol. 8, no. 1, pp. 21–28, 1962.
- [23] “Digital video broadcasting (DVB); Second generation framing structure, channel coding and modulation systems for broadcasting, interactive services, news gathering and other broad-band satellite applications,” EN 302 307, European Telecommunications Standards Institute (ETSI).
- [24] T. Richardson and S. Kudekar, “Design of low-density parity check codes for 5G new radio,” *IEEE Communications Magazine*, vol. 56, no. 3, pp. 28–34, 2018.
- [25] F. R. Kschischang, B. J. Frey, and H.-A. Loeliger, “Factor graphs and the sum-product algorithm,” *IEEE Transactions on information theory*, vol. 47, no. 2, pp. 498–519, 2001.
- [26] M. G. Luby, M. Mitzenmacher, M. A. Shokrollahi, and D. A. Spielman, “Efficient erasure correcting codes,” *IEEE Transactions on Information Theory*, vol. 47, no. 2, pp. 569–584, 2001.
- [27] —, “Improved low-density parity-check codes using irregular graphs,” *IEEE Transactions on information Theory*, vol. 47, no. 2, pp. 585–598, 2001.
- [28] T. J. Richardson and R. L. Urbanke, “The capacity of low-density parity-check codes under message-passing decoding,” *IEEE Transactions on information theory*, vol. 47, no. 2, pp. 599–618, 2001.

- [29] T. J. Richardson, M. A. Shokrollahi, and R. L. Urbanke, “Design of capacity-approaching irregular low-density parity-check codes,” *IEEE transactions on information theory*, vol. 47, no. 2, pp. 619–637, 2001.
- [30] D. Poulin and Y. Chung, “On the iterative decoding of sparse quantum codes,” *arXiv preprint arXiv:0801.1241*, 2008.
- [31] Z. Babar, P. Botsinis, D. Alanis, S. X. Ng, and L. Hanzo, “Fifteen years of quantum LDPC coding and improved decoding strategies,” *IEEE Access*, vol. 3, pp. 2492–2519, 2015.
- [32] N. Raveendran and B. Vasić, “Trapping sets of quantum LDPC codes,” *Quantum*, vol. 5, p. 562, 2021.
- [33] Y.-J. Wang, B. C. Sanders, B.-M. Bai, and X.-M. Wang, “Enhanced feedback iterative decoding of sparse quantum codes,” *IEEE transactions on information theory*, vol. 58, no. 2, pp. 1231–1241, 2012.
- [34] A. Rigby, J. Olivier, and P. Jarvis, “Modified belief propagation decoders for quantum low-density parity-check codes,” *Physical Review A*, vol. 100, no. 1, p. 012330, 2019.
- [35] Y.-H. Liu and D. Poulin, “Neural belief-propagation decoders for quantum error-correcting codes,” *Physical review letters*, vol. 122, no. 20, p. 200501, 2019.
- [36] X. Xiao, N. Raveendran, and B. Vasić, “Neural-net decoding of quantum LDPC codes with straight-through estimators,” in *in Proc. Information Theory and Applications Workshop (ITA)*, 2019.
- [37] S. Miao, A. Schnerring, H. Li, and L. Schmalen, “Neural belief propagation decoding of quantum LDPC codes using overcomplete check matrices,” in *2023 IEEE Information Theory Workshop (ITW)*. IEEE, 2023, pp. 215–220.
- [38] J. Old and M. Rispler, “Generalized belief propagation algorithms for decoding of surface codes,” *Quantum*, vol. 7, p. 1037, 2023.
- [39] K.-Y. Kuo and C.-Y. Lai, “Exploiting degeneracy in belief propagation decoding of quantum codes,” *npj Quantum Information*, vol. 8, no. 1, p. 111, 2022.
- [40] J. Du Crest, M. Mhalla, and V. Savin, “Stabilizer inactivation for message-passing decoding of quantum LDPC codes,” in *2022 IEEE Information Theory Workshop (ITW)*. IEEE, 2022, pp. 488–493.

- [41] M. Mézard, G. Parisi, and R. Zecchina, “Analytic and algorithmic solution of random satisfiability problems,” *Science*, vol. 297, no. 5582, pp. 812–815, 2002.
- [42] A. Montanari, F. Ricci-Tersenghi, and G. Semerjian, “Solving constraint satisfaction problems through belief propagation-guided decimation,” *arXiv preprint arXiv:0709.1667*, 2007.
- [43] A. Coja-Oghlan, “On belief propagation guided decimation for random  $k$ -SAT,” in *Proceedings of the twenty-second annual ACM-SIAM symposium on discrete algorithms*. SIAM, 2011, pp. 957–966.
- [44] T. Filler and J. Fridrich, “Binary quantization using belief propagation with decimation over factor graphs of LDGM codes,” *arXiv preprint arXiv:0710.0192*, 2007.
- [45] V. Aref, N. Macris, and M. Vuffray, “Approaching the rate-distortion limit with spatial coupling, belief propagation, and decimation,” *IEEE Transactions on Information Theory*, vol. 61, no. 7, pp. 3954–3979, 2015.
- [46] A. Buchberger, C. Häger, H. D. Pfister, L. Schmalen, and A. G. i Amat, “Learned decimation for neural belief propagation decoders,” in *ICASSP 2021-2021 IEEE International Conference on Acoustics, Speech and Signal Processing (ICASSP)*. IEEE, 2021, pp. 8273–8277.
- [47] R. E. Blahut, *Algebraic Codes for Data Transmission*. Cambridge University Press, 2003, ISBN-10 0521553741.
- [48] A. R. Calderbank and P. W. Shor, “Good quantum error-correcting codes exist,” *Physical Review A*, vol. 54, no. 2, p. 1098, 1996.
- [49] A. Steane, “Multiple-particle interference and quantum error correction,” *Proceedings of the Royal Society of London. Series A: Mathematical, Physical and Engineering Sciences*, vol. 452, no. 1954, pp. 2551–2577, 1996.
- [50] P. Iyer and D. Poulin, “Hardness of decoding quantum stabilizer codes,” *IEEE Transactions on Information Theory*, vol. 61, no. 9, pp. 5209–5223, 2015.
- [51] E. Berlekamp, R. McEliece, and H. Van Tilborg, “On the inherent intractability of certain coding problems (corresp.),” *IEEE Transactions on Information Theory*, vol. 24, no. 3, pp. 384–386, 1978.



- [52] J. Pearl, “Reverend Bayes on inference engines: A distributed hierarchical approach,” in *Proceedings of the Second National Conference on Artificial Intelligence*, 1982, pp. 133–136.
- [53] ———, *Probabilistic Reasoning in Intelligent Systems: Networks of Plausible Inference (2nd ed.)*. San Francisco, CA: Morgan Kaufmann, 1988.
- [54] C. Berrou, A. Glavieux, and P. Thitimajshima, “Near Shannon limit error-correcting coding and decoding: Turbo-codes. 1,” in *Proceedings of ICC’93-IEEE International Conference on Communications*, vol. 2. IEEE, 1993, pp. 1064–1070.
- [55] R. J. McEliece, D. J. C. MacKay, and J.-F. Cheng, “Turbo decoding as an instance of Pearl’s “belief propagation” algorithm,” *IEEE Journal on selected areas in communications*, vol. 16, no. 2, pp. 140–152, 1998.
- [56] S. M. Aji and R. J. McEliece, “The generalized distributive law,” *IEEE transactions on Information Theory*, vol. 46, no. 2, pp. 325–343, 2000.
- [57] M. Mézard and G. Parisi, “The Bethe lattice spin glass revisited,” *The European Physical Journal B-Condensed Matter and Complex Systems*, vol. 20, pp. 217–233, 2001.
- [58] J. Roffe, D. R. White, S. Burton, and E. Campbell, “Decoding across the quantum low-density parity-check code landscape,” *Physical Review Research*, vol. 2, no. 4, p. 043423, 2020.
- [59] E. Sharon, S. Litsyn, and J. Goldberger, “Efficient serial message-passing schedules for LDPC decoding,” *IEEE Transactions on Information Theory*, vol. 53, no. 11, pp. 4076–4091, 2007.
- [60] J. Goldberger and H. Kfir, “Serial schedules for belief-propagation: analysis of convergence time,” *IEEE Transactions on Information Theory*, vol. 54, no. 3, pp. 1316–1319, 2008.
- [61] K.-Y. Kuo and C.-Y. Lai, “Refined belief propagation decoding of sparse-graph quantum codes,” *IEEE Journal on Selected Areas in Information Theory*, vol. 1, no. 2, pp. 487–498, 2020.
- [62] C.-Y. Lai and K.-Y. Kuo, “Log-domain decoding of quantum LDPC codes over binary finite fields,” *IEEE Transactions on Quantum Engineering*, vol. 2, pp. 1–15, 2021.